Article

Production of Organizational Chiral Structures by Design

Audrey R. Sulkanen, Minyuan Wang, Logan A. Swartz, Jaeuk Sung, Gang Sun, Jeffrey S. Moore, Nancy R. Sottos,* and Gang-yu Liu*

Cite This: *J. Am. Chem. Soc.* 2022, 144, 824−831

Read Online

ACCESS | 📊 Metrics & More | 📰 Article Recommendations

ABSTRACT: Organizational chirality on surfaces has been of interest in chemistry and materials science due to its scientific importance as well as its potential applications. Current methods for producing organizational chiral structures on surfaces are primarily based upon the self-assembly of molecules. While powerful, the chiral structures are restricted to those dictated by surface reaction thermodynamics. This work introduces a method to create organizational chirality by design with nanometer precision. Using atomic force microscopy-based nanolithography, in conjunction with chosen surface chemistry, various chiral structures are produced with nanometer precision, from simple spirals and arrays of nanofeatures to complex and hierarchical chiral structures. The size, geometry, and organizational chirality is achieved in deterministic fashion, with high fidelity to the designs. The concept and methodology reported here provide researchers a new and generic means to carry out organizational chiral chemistry, with the intrinsic advantages of chiral structures by design. The results open new and promising applications including enantioselective catalysis, separation, and crystallization, as well as optical devices requiring specific polarized radiation and fabrication and recognition of chiral nanomaterials.
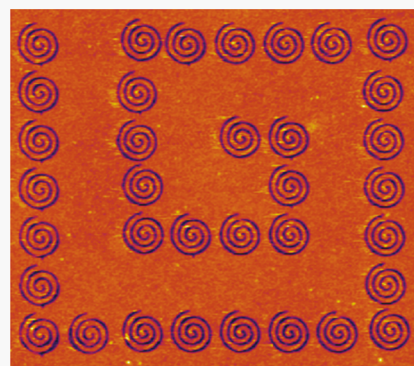
INTRODUCTION

Surface chirality is an area of growing interest, due to its intriguing scientific significance and many potential applications, such as chiral sensors, circularly polarized light emission, enantioselective separation, crystallization, and catalysis.[1−4] In addition to the well-known molecular chirality, surface chirality can also arise from achiral molecules, as certain absorbed conformations induce chirality.[5,6] A less studied form of surface chirality is organizational chirality, which arises solely from the arrangement of the molecules on the surface.[7] Therefore, both chiral[8,9] and achiral molecules[7,10−14] have been utilized to form organizational chiral structures. Current means to produce organizational chirality primarily rely on self-assembly, from simple and small organic molecules[7,9,15] to large aromatic ones.[13,16] The resulting chiral structures are restricted to those driven by the resulting intermolecular and molecule−surface interactions.

In order to go beyond this restriction and achieve organizational chirality deterministically, we turn to the combination of atomic force microscopy (AFM) and surface chemistry. Taking full advantage of the high spatial precision of AFM in performing nanolithography to create chiral geometries,[10,17−19] various functionalities and complex chiral designs are achieved. Multiple surface reactions were tested, including thiol adsorption on precious metals[20−24] and retro-Diels−Alder reactions of maleimide anthracene (MA) mechanophores.[25−29] Various chiral structures have been designed and produced with nanometer precision, from simple chiral spirals to arrays of chiral nanofeatures to hierarchical chiral structures where both the individual features and the overall layout are chiral. In addition to nanolithography, AFM also provides a powerful and high-resolution readout of molecular assemblies on surfaces[25,30,31] and, therefore, was utilized in this work to reveal organizational chiral features produced. The concept and methodology reported here enable a new and generic means to perform organizational chiral chemistry, with the intrinsic advantages of creating structures by design. The results reported here open new and promising applications including organizational chiral sensors, 3D chiral nanoprinting, enantiomeric separation, and enantiomeric heterogeneous catalysis.
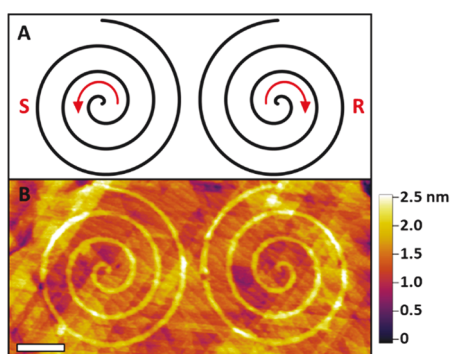
RESULTS AND DISCUSSION

Production of Organizational Chiral Structures Using Nanolithography and Surface Chemisorption. To demonstrate that AFM-based nanolithography enables production of organizational chiral structures, we first designed a pair of simple Archimedean spirals, as shown in Figure 1A. The
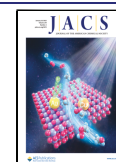
Figure 1. (A) Design of a pair of S and R spirals. (B) AFM topographic image (1.5 μm × 0.75 μm) of the pair of chiral structures produced following A. Image was acquired in a 0.02 mM C_{18} ethanol solution under a force of 6.7 nN and a scanning speed of 3.76 μm/s. Lateral scale bar = 0.2 μm.

spiral on the left rotates counterclockwise outward from the center, thus is denoted as "S" chirality. Its mirror image on the right thus exhibits "R" chirality. The chirality is further verified by the lack of improper rotational symmetry in each feature; that is, neither spiral is superimposable on its mirror image within the plane.

Translating the design into true chemical features requires selecting the appropriate surface chemistry, scaling the design to the desired size, setting the nanolithography conditions, and finally performing the AFM-based nanolithography accordingly. In Figure 1, this was done by nanografting.[18,30] In summary, a 1-octanethiol (abbreviated as C_8) self-assembled monolayer (SAM), created on an ultraflat Au thin film,[30] was used as the matrix or canvas. 1-Octadecanethiol (abbreviated as C_{18}) molecules were used as the active component for the spirals. The C_8 SAM was first imaged via AFM in a solution of 0.02 mM C_{18} in ethanol under a low force of 6.7 nN, from which the nanolithography site was chosen. The design (shown in Figure 1A) can be created using any graphic software, in this case, simply MS-PowerPoint, and saved in png format. It was then read and displayed directly by our AFM data acquisition program on the acquired AFM image. The displayed spirals were then moved to the designated location and scaled to the desired size. The spirals are Archimedean spirals defined by eqs 1 and 2

$$r \text{ (nm)} = 18.00 \text{ (nm)} \times \theta \tag{1}$$

$$r \text{ (nm)} = -18.00 \text{ (nm)} \times \theta \tag{2}$$

where r is the distance from the spiral's center, the two coefficients (18 and −18) are the Archimedean constant and dictate the chirality (e.g., positive values yield S-chirality) and spacing between orders of the contours, and θ is the counterclockwise angle measured with respect to the horizontal axis. Equations 1 and 2 describe the S and R spirals in Figure 1A, respectively, with a range of θ from 0 to 6.5 π. Setting the nanografting force to 218 nN, the AFM tip was then scanned at 1.0 μm/s at this high load, tracing the contours of the displayed spirals. The high force shaved the C_8 from the Au surface, and the void was then immediately filled by the C_{18} molecules in the imaging medium. After nanografting, the 1.5 μm × 0.75 μm area was imaged at a much-reduced force of 6.7 nN. As shown in Figure 1B, the two spirals were faithfully produced, quantified by eqs 3 and 4 below:

$$r \text{ (nm)} = 18.10 \text{ (nm)} \times \theta \tag{3}$$

$$r \text{ (nm)} = -17.82 \text{ (nm)} \times \theta \tag{4}$$

where θ ranged from 0 to 6.5 π, agreeing with the designed size in eqs 1 and 2 with nanometer precision. The height of C_{18} measured 0.7 ± 0.2 nm above the surrounding C_8 SAM, consistent with the known SAM structure of closely packed alkanethiol molecules whose chains are tilted 30° from the surface normal.[22,32,33] The S spiral had three rotations, with the line width (defined as the full-width at half-maximum, fwhm) measured as 24.9 ± 1.5 nm, separated by 104.2 ± 3.8 nm between successive orders of contours. Although alkanethiols are achiral molecules, both C_{18} spirals, by definition, exhibit S and R organizational chirality, respectively.[7]

For AFM instruments without the capability of using polar coordinates or uploading graphic designs, one could easily produce chiral features by defining the specific values in the X and Y scanning directions. Using Archimedean spirals as an example, the XY positions of the spiral follow the parametric eqs 5 and 6:

$$X \text{ (nm)} = a \text{ (nm)} \times \theta \times \cos(\theta) \tag{5}$$

$$Y \text{ (nm)} = a \text{ (nm)} \times \theta \times \sin(\theta) \tag{6}$$

where X and Y represent the coordinates of the designed structure, a is a scaling factor whose sign determines the chirality of the spiral, and θ determines the number of rotations of the spiral.

A specific design and its nanoscale rendition are shown in Figure 2, where the nanografting was performed following the designed parametric equations. This Archimedean S spiral is represented and quantified using eqs 7 and 8:

$$X \text{ (nm)} = 13.32 \text{ (nm)} \times \theta \times \cos(\theta) \tag{7}$$

$$Y \text{ (nm)} = 13.32 \text{ (nm)} \times \theta \times \sin(\theta) \tag{8}$$

where the variable θ ranged from 0 to 31.8 π with increments of 0.318 π. Setting the shaving force to 218 nN, the equations were entered into the AFM scanning commands. During the scan at 1.0 μm/s, the spiral path was traced under 218 nN, according to XY positions defined by eqs 7 and 8 (shown in Figure 2A). Again, nanografting took place, where the C_8 molecules were replaced by C_{18} molecules from the solution of 0.02 mM C_{18} in ethanol. The resulting feature is revealed in Figure 2B, where the S spiral had 16 rotations, with a line width equal to 23.5 ± 0.0 nm, separated by 83.9 ± 2.9 nm between successive orders of contours. The height of the spiral was 0.9 ± 0.1 nm above its surrounding C_8 SAM, which is consistent with the expected height difference between the C_{18} and C_8 SAMs shown schematically in Figure 2C.[34]

Complementary to scanning electron microscopy (SEM)-based lithography, which can reach similar length scales and precision, AFM nanolithography offers additional capabilities to produce features through additive, subtractive, and reactive means. Additionally, our methodology enables production of designed functionalities under wet chemistry environments (while SEM requires high vacuum), offering high versatility in chemistry and materials science.

Compared with prior approaches of producing organizational chiral structures,[35−39] our method allows deterministic production of organizational chiral structures instead of being restricted to simple structures dictated by reaction thermodynamics. The spatial precision of AFM enables nanometer
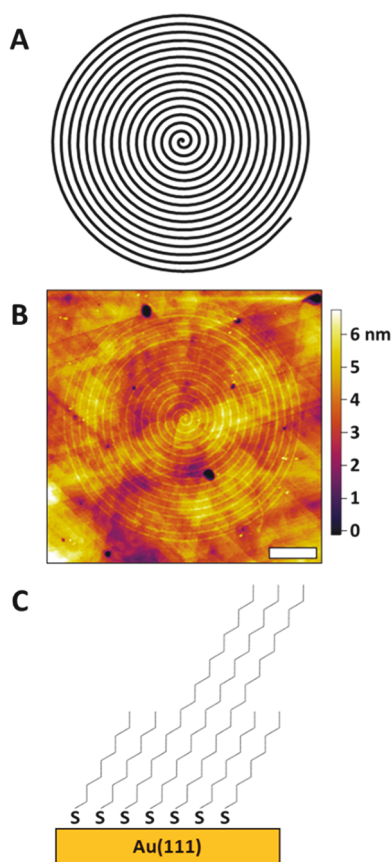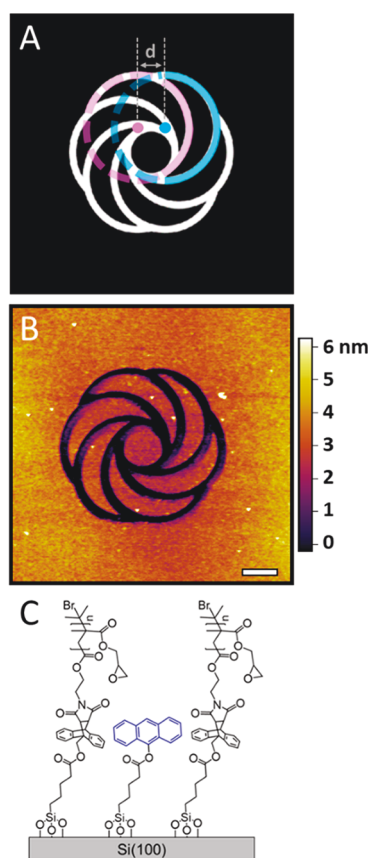
Figure 2. (A) *S* spiral defined by the parametric eqs 7 and 8. (B) 3.0 μm × 3.0 μm AFM topographic image containing the *S* spiral of C_{18} inlaid in a C_8 SAM. The AFM image was acquired in an ethanol solution containing 0.02 mM C_{18}, under a force of 6.7 nN and at a speed of 7.52 μm/s. Lateral scale bar = 0.5 μm. (C) Schematic diagram of nanografted C_{18} inlaid in C_8 SAM revealing the adsorption conformation of the alkanethiols.

Figure 3. (A) Design of a six-bladed fan feature with *R*-chirality. (B) 7 μm × 7 μm AFM topographic image taken after production of the *R*-bladed fan shown in A. The image was acquired in DMSO under an imaging force of 18 nN at 17.53 μm/s. Scale bar = 1.0 μm. (C) Schematic diagram illustrating the molecular adsorbates and terminal functionalities across the patterned region.

resolution in both production and imaging.[24,31,40] The organizational chirality, feature geometry, and overall feature size followed the intended designs faithfully. Combined with the recent advances in SAM chemistry,[21,41−46] this approach can accommodate a wide range of material and functionality. Example head-groups include thiols,[30] dithiols,[47] disulfides,[48] alkynes,[49] and silane chemistries,[50] with terminal groups of COOH, CHO, NH_2, biotin, and the like.[34,44−46,51,52]

The organizational chiral structures created here can be used as templates to selectively attract macromolecules with desired chiralities, e.g., *R* or *S*, onto surfaces.[36,53]

Production of Organizational Chiral Structures Using Nanolithography and Mechanochemistry. Expanding our designs beyond simple Archimedean spirals, a bladed fan feature is shown in Figure 3A with features illustrating how an *R*-bladed fan design is generated. Each of the "blades" are produced by a nonoverlapping region of two equal sized circles (e.g., blue and pink in Figure 3A). The diameter of the circles, *D*, and the separation between their centers, *d*, determine the overall size and geometry of each "blade". Neighboring "blades" are rotated 60° with respect to each other, with a shared side and a shared point, thus creating this six-bladed fan feature.

Utilizing mechanochemistry[26,54,55] of an interfacial MA mechanophore system,[25,27] we produced a six-bladed fan

consisting of anthracene termini on Si wafers, as shown in Figure 3. To create this feature, a siloxane SAM was first produced on a Si(100) surface following procedures previously reported.[25] Each covalently bound molecule contained a MA mechanophore and was terminated by a poly(glycidyl methacrylate) (PGMA) tail. This thin film was imaged via AFM in dimethyl sulfoxide (DMSO) under a low force of 18 nN to enable selection of sites for nanofabrication. The design in Figure 3A was exported as a bitmap image and directly uploaded into our AFM data acquisition software for displaying and sizing. With the black contrast set to 30 nN and bright contrast set to 800 nN, the AFM scanned the blade pattern with the defined forces. The results are shown in Figure 3B, where the blades are clearly visible, appearing as negative contrast in the AFM topograph. The *R* chiral structure followed the design pattern with high fidelity. The parent circles had *D* = 3.43 ± 0.15 μm, with a center−center separation of *d* = 0.79 ± 0.08 μm. The width of the blade lines at fwhm was 0.23 ± 0.07 μm, while the diameter of the central circle was 1.15 ± 0.07 μm. The anthracene termini regions were 3.83 ± 0.39 nm lower than that of the surrounding polymer brush. This structure is consistent with the activation of the MAs under the high force via the retro-Diels−Alder reaction, followed by the departure of PGMA groups, the results of which are shown schematically in Figure 3C.[25]

While the reactions used in Figures 1 and 2 were adsorption directed by AFM scans, the reactions achieved in Figures 3 and 4 were based on detachment of PGMA tails by the local force
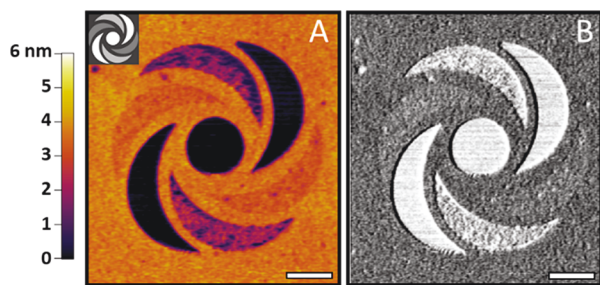
Figure 4. (A) AFM topographic image taken after scanning the chiral grayscale image inset on an MA surface. (B) Lateral image acquired simultaneously. Images were collected in DMSO under 70 nN and at a speed of 22.54 μm/s. Scale bars = 1.0 μm.

exerted via the AFM probe. The later enables production of multicontrast organizational chiral features, as illustrated in Figure 4. A multicontrast R-bladed fan was designed and produced. Modifying the design in Figure 3, the fan in Figure 4 has six solid and well-separated blades, with each pair of opposite blades assigned a contrast in gray scale (Figure 4A, inset). Setting the shaving force, based on blade contrast in the design, to be 333, 617, and 900 nN for dark, gray, and bright, respectively, the AFM probe was able to activate the MA groups in the blade regions. The number of MA groups activated was based on the force setting,[25] resulting in the complex, multicontrast organizational chiral structure shown in Figure 4A. The diameter, D, of the parent circles measured 3.79 ± 0.04 μm with a center−center separation $d = 0.97 ± 0.03$ μm. The diameter of the central circle was 1.28 ± 0.02 μm, with a depth of 7.0 nm. The depths of each "blade" feature were 1.27 ± 0.31, 4.43 ± 1.88, and 7.46 ± 0.09 nm lower than the surroundings, corresponding to MA activation densities of 17 ± 4%, 58 ± 25%, and 98 ± 1%, respectively. In addition to the morphological changes revealed in AFM, fluorescence imaging also provided corroborative evidence as the intensity correlates to the surface concentration of the resulting anthracene termini.[25,28] Additional supportive evidence arises from the lateral image, shown in Figure 4B. The lateral image was acquired simultaneously with the AFM topograph. The lateral image contrast is opposite that of the topographic image, as the lateral force in the anthracene regions is higher than that in the bromide-terminated regions.[25]

In organizational chiral structures reported in the past, self-assembly was primarily utilized, in which the area and chirality are determined by the interplay between thermodynamics and kinetics. This resulted in domains of finite size occupied by one enantiomeric form of the chiral features,[6,9,16,56−58] while the entire surface is covered by interspaced pockets of segregated chiral structures.[9,11,13,35,57,59,60] Our approach is capable of tiling large surface areas with a homogeneous enantiomeric form by design, which brings organizational chiral structures to a new scientific level and closer to practical applications.[61] Figure 5 demonstrates the feasibility to produce arrays of enantioselective chiral features at designated surface locations. A 3 × 3 array of R-bladed fans was designed and produced, following similar protocols to that in Figure 3. The periodicity of the 3 × 3 array measured 1.69 ± 0.01 μm, and all of the individual features within the array were R-bladed fans. The
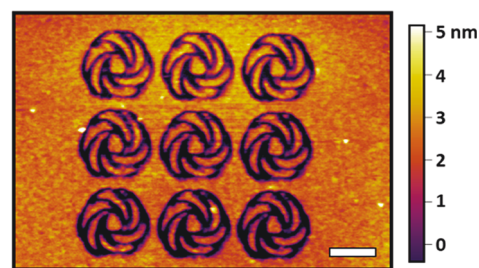
Figure 5. AFM topographic image of a 3 × 3 array of chiral structures produced using the protocols from Figure 3. Each chiral structure is a six-bladed fan with R-chirality. Dark features correspond to anthracene termini, while the lighter features are the bromide termini of the PGMA chains. The image was acquired in DMSO under an imaging force of 18 nN at 17.52 μm/s. Scale bar = 1.0 μm.

parent circles D measured 0.90 ± 0.03 μm, with a center−center separation of $d = 0.27 ± 0.02$ μm. The width of the blade lines at the fwhm was 0.13 ± 0.01 μm, while the lateral dimension of the central region was 0.28 ± 0.01 μm.

Patterning surfaces with arrays of organizational chiral features enables regulation of the electroclinic effect, as well as regulating chiral optical properties of thin film materials.[10] The current AFM instrument used for this investigation has the capability to produce chiral features covering an entire 100 μm × 100 μm area in a single scan frame. By utilizing manual manipulation via a precision micrometer to pattern adjacent 100 μm × 100 μm areas, coverage of millimeter-sized surfaces is achievable.

Production of Hierarchical Chiral Structures. Taking full advantage of this technology's capability to make organizational chiral structures by design, we produced hierarchical chiral structures where the individual structures and their arrangement are both chiral. Figure 6A provides an example hierarchical chiral structure where each element is an Archimedean spiral with R-chirality, and the spirals are arranged periodically along a rectangular spiral, also with R-chirality. This design is referred to as an $\mathbf{R}^{\mathbf{R}}$ structure, where $\mathbf{R}$ represents the chirality of the individual elements, and the superscript $^{\mathbf{R}}$ denotes the chirality of their arrangement. All trajectories were generated using MS-PowerPoint and saving in png format. The png file was then uploaded and placed on an acquired AFM image of the chosen surface region. Finally, the feature was positioned and resized in reference to the actual surface region to our desired location and dimensions.

The final design of individual Archimedean spirals is similar to that in Figure 1A, i.e., R-chirality, and quantified by eq 9:

$$r \ (\text{nm}) = -29.00 \ (\text{nm}) \times \theta \tag{9}$$

with θ ranging from 0 to 6.5 π. There are 35 Archimedean spirals in this design, whose centers were arranged following the trajectory of the red rectangular spiral with a periodicity of 1.30 μm, illustrated in Figure 6A. The first segment of the rectangular spiral had one period, followed by a 90° right turn, and increased by one period for each subsequent segment. Figure 6B shows the results of the AFM-directed nanolithography following the design in Figure 6A, using the protocols similar to that described in Figure 1 on a MA substrate. The individual Archimedean spirals followed the design faithfully, with the spirals defined by eq 10:

$$r \ (\text{nm}) = (-29.26 ± 3.71 \ \text{nm}) \times \theta \tag{10}$$
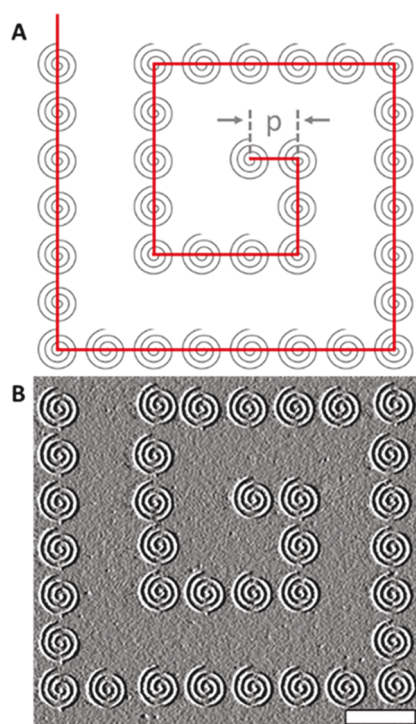
Figure 6. (A) Design of an R^R hierarchical spiral. (B) 11.4 μm × 10.1 μm deflection image of the R^R hierarchical spiral produced following the design in A. The image was acquired in DMSO under an imaging force of 51 nN at 37.56 μm/s. The lateral scale bar = 2.0 μm.

with θ ranging from 0 to 6.5 π. The width of the spiral lines at fwhm was 96.07 ± 13.58 nm. These Archimedean spirals were aligned along the R-rectangular spiral with the periodicity, p, measured as 1.33 ± 0.03 μm. The Archimedean spiral lines correspond to the anthracene-terminated areas, which measured 5.21 ± 0.78 nm lower than the surrounding from AFM topographic images, consistent with the activation of the MA mechanophores.[25] In the AFM deflection image shown in Figure 6B, the bright contrast corresponds to the anthracene functionality, while the surroundings are the bromide termini of the PGMA chains.

To demonstrate the robustness of the concept of "producing hierarchical chiral structures by design", we have completed the design and production of all four possible combinations of chirality associated with Figure 6, i.e., R^R, R^S, S^R, and S^S. The results of all four types of hierarchical chiral structures are shown in Figure 7 and summarized in Table 1. The fidelity is very high in this AFM-based nanolithography. Using the R^R spiral as an example, the alignment of the spirals was within 16.7 ± 48.7 nm of the intended rectangular spiral line and the periodicity is preserved within tens of nanometers (see Table 1) of the design. The other three hierarchical spiral features had similar levels of precise alignment, demonstrating that all configurations can be successfully and precisely produced.

■ CONCLUSIONS

This work introduces our approach to create organizational chiral structures with nanometer precision by design. Current methods for production of organizational chirality are primarily based upon self-assembly of molecules. While powerful, the chiral structures and the size of the assemblies produced are restricted to those dictated by reactions thermodynamics. Using AFM in conjunction with chosen surface reactions, our
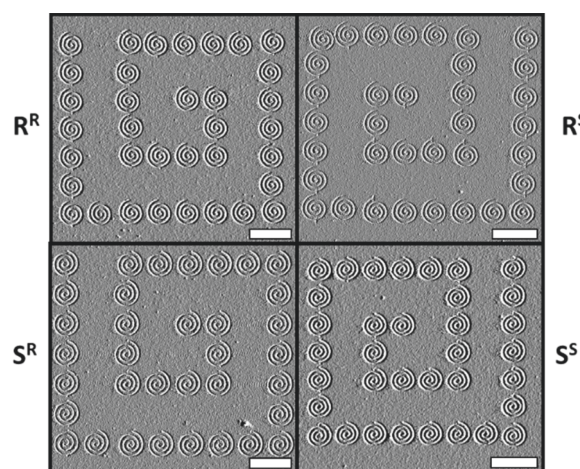
Figure 7. Four AFM deflection images of the hierarchical chiral spirals produced following the designs. All images were acquired in DMSO under the imaging forces of 51, 13, 47, and 23 nN, with the scanning speeds of 37.56, 31.30, 35.06, and 32.55 μm/s, respectively, in the four experiments. All lateral scale bars = 2.0 μm.

Table 1. Summary of Hierarchical Chiral Spirals Produced, Representing All Four Possible Combinations of Chirality[a]

Hierarchical Chirality	R^R	R^S	S^R	S^S
Archimedean Spirals Produced				
Equation form of the Archimedean spirals produced	$r = \theta \times$ (-28.25 ± 1.24)	$r = \theta \times$ (-26.90 ± 1.98)	$r = \theta \times$ (29.60 ± 0.58)	$r = \theta \times$ (25.54 ± 0.74)
θ Range	0 to 6.5 π	0 to 6.5 π	0 to 6.5 π	0 to 6.5 π
Line width (nm)	96.07 ± 13.58	88.05 ± 15.45	98.64 ± 17.33	91.58 ± 12.91
Height difference after MA activation (nm)	5.21 ± 0.78	6.10 ± 0.78	5.26 ± 1.46	6.33 ± 1.11
Alignment of Archimedean Spirals Along the Rectangular Spiral				
Periodicity, p (μm)	1.33 ± 0.03	1.27 ± 0.02	1.46 ± 0.0.08	1.22 ± 0.02

[a]The measurements are derived from AFM topographic as well as deflection images.

methodology enables production of various chiral structures with nanometer precision, from simple chiral spirals to arrays of chiral nanofeatures, to hierarchical chiral structures. The size, geometry, and organizational chirality followed the designs with a high degree of spatial fidelity. The individual chiral structures, their locations on surfaces, and total coverage of these organizational chiral structures were controlled. The ability to selectively produce a single chiral form is crucial to facilitating enantioselective surface reactions. This approach will enhance additive manufacturing by enabling 3D chiral nanoprinting, via integrated microfluidic delivery with AFM.[40,62,63] By employing parallel processing techniques,[61] the throughput of making organizational chiral structures by design can be greatly increased, making it feasible to scale up. The results open new and promising applications including organizational chiral sensors, enantiomeric separation, and enantiomeric heterogeneous catalysis.

EXPERIMENTAL METHODS AND MATERIALS

Materials. Chemical reagents were used without further purification unless specifically stated. Ethanol (200 proof) was purchased from VWR (Radnor, PA, USA). Gold slugs (99.999% pure) were purchased from Alfa Aesar (Haverhill, MA, USA). Mica sheets were purchased from S & J Trading Inc. (Glen Oaks, NY, USA). Deionized and ultrapure water with a resistivity of 18.2 MΩ·cm at 25 °C was generated by a Milli-Q water system (EMD Millipore, Billerica, MA, USA). Dimethyl sulfoxide (99.9%), N,N,N',N'',N''-pentamethyldiethylenetriamine (PMDETA) (99%), glycidyl methacrylate (97.0%), sulfuric acid (95%), hydrogen peroxide (30% aqueous solution), ethyl-2-bromoisobutyrate, and copper(II) bromide (99%) were obtained from Sigma-Aldrich (St. Louis, MO, USA). 1-Octanethiol (≥98.5%) and 1-octadecanethiol (98%) were purchased from Sigma-Aldrich (St. Louis, MO, USA). Polished silicon wafers, Si(100), were purchased from University Wafers Inc. (Boston, MA, USA). Silicon cantilevers (AC-240, spring constant, $k = 1.7$ N/m) were procured from Olympus America (Central Valley, PA, USA). Silicon nitride cantilevers (MSNL-10, $k = 0.6$ N/m) were procured from Bruker Nano (Camarillo, CA, USA).

Preparation of Self-Assembled Monolayers on Surfaces. Ultraflat gold thin films were prepared based on previously published methods.[30] Self-assembled monolayers were formed by soaking the gold thin films in 1.0 mM C_8 thiol in ethanol solutions. The substrates remained in these solutions until being used for nanografting to ensure high coverage and minimal contamination.

MA mechanophore samples were prepared according to previously published methods.[25] In brief, active specimens of maleimide–anthracene mechanophores with bromoisobutyrate terminal functionalization were immobilized on Si(100) surfaces. After functionalization, the PGMA polymer brush was grown from the bromoisobutyrate group via a copper-catalyzed living radical polymerization of glycidyl methacrylate.

High-Resolution AFM Imaging and Nanolithography. A deflection-type AFM (MFP-3D, Oxford Instrument, Santa Barbara, CA, USA) was used for nanolithography and high-resolution imaging. Data acquisition was carried out using MFP-3D software developed based on the Igor Pro 6.34 platform. The basic protocol of nanografting has been reported previously.[18,30] Briefly, SAMs were first imaged using a silicon nitride cantilever with a low force in contact mode in a solution of C_{18} in ethanol. After selecting a desired region, nanolithography was done by applying a high force to the AFM tip (indicated for each figure) and tracing the desired pattern. After the lithography scans, the areas were scanned again with a low force to visualize the lithography results. Data analysis is done using the MFP-3D's Igor Pro 6.34 software. The results are shown in Figures 1 and 2. Imaging and nanofabrication conditions varied and are provided for each experiment.

For the MA mechanophore AFM images shown in Figures 3–7, a protocol similar to previously published methods was used.[25] The silicon cantilevers were used in contact mode in DMSO for imaging and nanolithography. Imaging and nanofabrication conditions varied and are provided for each experiment.

AUTHOR INFORMATION

Corresponding Authors

Nancy R. Sottos — *Materials Science and Engineering and Beckman Institute for Advanced Science and Technology, University of Illinois Urbana–Champaign, Urbana, Illinois 61801, United States;* orcid.org/0000-0002-5818-520X; Email: n-sottos@illinois.edu

Gang-yu Liu — *Department of Chemistry, University of California, Davis, California 95616, United States; Agricultural and Environmental Chemistry Graduate Group and Biophysics Graduate Group, University of California, Davis, California 95616, United States;* orcid.org/0000-0003-3689-0685; Email: gyliu@ucdavis.edu

Authors

Audrey R. Sulkanen — *Department of Chemistry, University of California, Davis, California 95616, United States;* orcid.org/0000-0002-7863-2484

Minyuan Wang — *Agricultural and Environmental Chemistry Graduate Group, University of California, Davis, California 95616, United States*

Logan A. Swartz — *Biophysics Graduate Group, University of California, Davis, California 95616, United States*

Jaeuk Sung — *Materials Science and Engineering and Beckman Institute for Advanced Science and Technology, University of Illinois Urbana–Champaign, Urbana, Illinois 61801, United States;* Present Address: Samsung Electronics, 1 Samsungjeonja-ro, Hwaseong-si, 18448, South Korea

Gang Sun — *Agricultural and Environmental Chemistry Graduate Group and Department of Biological and Agricultural Engineering, University of California, Davis, California 95616, United States;* orcid.org/0000-0002-6608-9971

Jeffrey S. Moore — *Materials Science and Engineering, Beckman Institute for Advanced Science and Technology, and Department of Chemistry, University of Illinois Urbana–Champaign, Urbana, Illinois 61801, United States;* orcid.org/0000-0001-5841-6269

Complete contact information is available at:
https://pubs.acs.org/10.1021/jacs.1c10491

Author Contributions

The manuscript was written through contributions of all authors. All authors have given approval to the final version of the manuscript.

Notes

The authors declare no competing financial interest.

ACKNOWLEDGMENTS

REFERENCES

(1) Deng, Y.; Wang, M.; Zhuang, Y.; Liu, S.; Huang, W.; Zhao, Q. Circularly polarized luminescence from organic micro-/nano-structures. *Light Sci. Appl.* **2021**, *10* (1), 76.

(2) Mallat, T.; Orglmeister, E.; Baiker, A. Asymmetric catalysis at chiral metal surfaces. *Chem. Rev.* **2007**, *107* (11), 4863–4890.

(3) Gellman, A. J. Chiral surfaces: accomplishments and challenges. *ACS Nano* **2010**, *4* (1), 5–10.

(4) Wang, C.; Hao, H.; Hashizume, D.; Tajima, K. Surface-induced enantiomorphic crystallization of achiral fullerene derivatives in thin films. *Chem. Sci.* **2020**, *11* (18), 4702–4708.

(5) Mark, A. G.; Forster, M.; Raval, R. Recognition and ordering at surfaces: the importance of handedness and footedness. *ChemPhysChem* **2011**, *12* (8), 1474–1480.

(6) Darling, G. R.; Forster, M.; Lin, C.; Liu, N.; Raval, R.; Hodgson, A. Chiral segregation driven by a dynamical response of the adsorption footprint to the local adsorption environment: bitartrate on Cu(110). *Phys. Chem. Chem. Phys.* **2017**, *19* (11), 7617–7623.

(7) Bombis, C.; Weigelt, S.; Knudsen, M. M.; Norgaard, M.; Busse, C.; Laegsgaard, E.; Besenbacher, F.; Gothelf, K. V.; Linderoth, T. R. Steering Organizational and Conformational Surface Chirality by

Controlling Molecular Chemical Functionality. *ACS Nano* **2010**, *4* (1), 297−311.

(8) Li, C.; Li, R.; Xu, Z.; Li, J.; Zhang, X.; Li, N.; Zhang, Y.; Shen, Z.; Tang, H.; Wang, Y. Packing Biomolecules into Sierpinski Triangles with Global Organizational Chirality. *J. Am. Chem. Soc.* **2021**, *143* (36), 14417−14421.

(9) Barlow, S. M.; Raval, R. Complex organic molecules at metal surfaces: bonding, organisation and chirality. *Surf. Sci. Rep* **2003**, *50* (6−8), 201−341.

(10) Pendery, J.; Ferjani, S.; Rosenblatt, C.; Petschek, R. G. Spatially controllable surface chirality at the nanoscale. *Epl-Europhys. Lett.* **2011**, *96* (2), 26001.

(11) Raval, R. Chiral expressions at metal surfaces. *Curr. Opin. Solid State Mater. Sci.* **2003**, *7* (1), 67−74.

(12) Cao, H.; Destoop, I.; Tahara, K.; Tobe, Y.; Mali, K. S.; De Feyter, S. Complex Chiral Induction Processes at the Solution/Solid Interface. *J. Phys. Chem. C Nanomater Interfaces* **2016**, *120* (31), 17444−17453.

(13) Liu, J.; Chen, T.; Deng, X.; Wang, D.; Pei, J.; Wan, L. J. Chiral hierarchical molecular nanostructures on two-dimensional surface by controllable trinary self-assembly. *J. Am. Chem. Soc.* **2011**, *133* (51), 21010−21015.

(14) Wang, Y. L.; Fabris, S.; Costantini, G.; Kern, K. Tertiary Chiral Domains Assembled by Achiral Metal-Organic Complexes on Cu(110). *J. Phys. Chem. C* **2010**, *114* (30), 13020−13025.

(15) Raval, R. Chiral expression from molecular assemblies at metal surfaces: insights from surface science techniques. *Chem. Soc. Rev.* **2009**, *38* (3), 707−721.

(16) Ecija, D.; Seufert, K.; Heim, D.; Auwarter, W.; Aurisicchio, C.; Fabbro, C.; Bonifazi, D.; Barth, J. V. Hierarchic self-assembly of nanoporous chiral networks with conformationally flexible porphyrins. *ACS Nano* **2010**, *4* (8), 4936−4942.

(17) Navikas, V.; Gavutis, M.; Rakickas, T.; Valiokas, R. N. Scanning Probe-Directed Assembly and Rapid Chemical Writing Using Nanoscopic Flow of Phospholipids. *ACS Appl. Mater. Interfaces* **2019**, *11* (31), 28449−28460.

(18) Xu, S.; Liu, G.-y. Nanometer-Scale Fabrication by Simultaneous Nanoshaving and Molecular Self-Assembly. *Langmuir: the ACS journal of surfaces and colloids* **1997**, *13* (2), 127−129.

(19) Xu, S.; Laibinis, P. E.; Liu, G.-y. Accelerating the Kinetics of Thiol Self-Assembly on GoldA Spatial Confinement Effect. *J. Am. Chem. Soc.* **1998**, *120* (36), 9356−9361.

(20) Bain, C. D.; Troughton, E. B.; Tao, Y. T.; Evall, J.; Whitesides, G. M.; Nuzzo, R. G. Formation of Monolayer Films by the Spontaneous Assembly of Organic Thiols from Solution onto Gold. *J. Am. Chem. Soc.* **1989**, *111* (1), 321−335.

(21) Love, J. C.; Estroff, L. A.; Kriebel, J. K.; Nuzzo, R. G.; Whitesides, G. M. Self-assembled monolayers of thiolates on metals as a form of nanotechnology. *Chem. Rev.* **2005**, *105* (4), 1103−1169.

(22) Xu, S.; Cruchon-Dupeyrat, S. J. N.; Garno, J. C.; Liu, G. Y.; Jennings, G. K.; Yong, T. H.; Laibinis, P. E. In situ studies of thiol self-assembly on gold from solution using atomic force microscopy. *J. Chem. Phys.* **1998**, *108* (12), 5002−5012.

(23) Karpovich, D. S.; Blanchard, G. J. Direct Measurement of the Adsorption-Kinetics of Alkanethiolate Self-Assembled Monolayers on a Microcrystalline Gold Surface. *Langmuir: the ACS journal of surfaces and colloids* **1994**, *10* (9), 3315−3322.

(24) Carpick, R. W.; Salmeron, M. Scratching the Surface: Fundamental Investigations of Tribology with Atomic Force Microscopy. *Chem. Rev.* **1997**, *97* (4), 1163−1194.

(25) Sulkanen, A. R.; Sung, J.; Robb, M. J.; Moore, J. S.; Sottos, N. R.; Liu, G.-y. Spatially Selective and Density-Controlled Activation of Interfacial Mechanophores. *J. Am. Chem. Soc.* **2019**, *141* (9), 4080−4085.

(26) Li, J.; Nagamani, C.; Moore, J. S. Polymer Mechanochemistry: From Destructive to Productive. *Acc. Chem. Res.* **2015**, *48* (8), 2181−2190.

(27) Li, J.; Shiraki, T.; Hu, B.; Wright, R. A.; Zhao, B.; Moore, J. S. Mechanophore activation at heterointerfaces. *J. Am. Chem. Soc.* **2014**, *136* (45), 15925−15928.

(28) Sung, J.; Robb, M. J.; White, S. R.; Moore, J. S.; Sottos, N. R. Interfacial Mechanophore Activation Using Laser-Induced Stress Waves. *J. Am. Chem. Soc.* **2018**, *140* (15), 5000−5003.

(29) Ghanem, M. A.; Basu, A.; Behrou, R.; Boechler, N.; Boydston, A. J.; Craig, S. L.; Lin, Y.; Lynde, B. E.; Nelson, A.; Shen, H.; Storti, D. W. The role of polymer mechanochemistry in responsive materials and additive manufacturing. *Nat. Rev. Mater.* **2021**, *6* (1), 84−98.

(30) Xu, S.; Miller, S.; Laibinis, P. E.; Liu, G. Y. Fabrication of nanometer scale patterns within self-assembled monolayers by nanografting. *Langmuir: the ACS journal of surfaces and colloids* **1999**, *15* (21), 7244−7251.

(31) Edwards, C. M.; Ulapane, S. B.; Kamathewatta, N. J. B.; Ashberry, H. M.; Berrie, C. L. Fabrication and Growth Control of Metal Nanostructures through Exploration of Atomic Force Microscopy-Based Patterning and Electroless Deposition Conditions. *J. Phys. Chem. C* **2020**, *124* (46), 25588−25601.

(32) Strong, L.; Whitesides, G. M. Structures of Self-Assembled Monolayer Films of Organosulfur Compounds Adsorbed on Gold Single-Crystals - Electron-Diffraction Studies. *Langmuir: the ACS journal of surfaces and colloids* **1988**, *4* (3), 546−558.

(33) Dubois, L. H.; Nuzzo, R. G. Synthesis, Structure, and Properties of Model Organic-Surfaces. *Annu. Rev. Phys. Chem.* **1992**, *43*, 437−463.

(34) Liu, M.; Amro, N. A.; Liu, G. Y. Nanografting for surface physical chemistry. *Annu. Rev. Phys. Chem.* **2008**, *59* (1), 367−386.

(35) Chen, T.; Wang, D.; Wan, L. J. Two-dimensional chiral molecular assembly on solid surfaces: formation and regulation. *National Science Review* **2015**, *2* (2), 205−216.

(36) Goronzy, D. P.; Ebrahimi, M.; Rosei, F.; Arramel; Fang, Y.; De Feyter, S.; Tait, S. L.; Wang, C.; Beton, P. H.; Wee, A. T. S.; Weiss, P. S.; Perepichka, D. F. Supramolecular Assemblies on Surfaces: Nanopatterning, Functionality, and Reactivity. *ACS Nano* **2018**, *12* (8), 7445−7481.

(37) Xu, Y.; Duan, J. J.; Yi, Z. Y.; Zhang, K. X.; Chen, T.; Wang, D. Chirality of molecular nanostructures on surfaces via molecular assembly and reaction: manifestation and control. *Surf. Sci. Rep* **2021**, *76* (3), 100531.

(38) Mali, K. S.; Pearce, N.; De Feyter, S.; Champness, N. R. Frontiers of supramolecular chemistry at solid surfaces. *Chem. Soc. Rev.* **2017**, *46* (9), 2520−2542.

(39) Zaera, F. Chirality in adsorption on solid surfaces. *Chem. Soc. Rev.* **2017**, *46* (23), 7374−7398.

(40) Zhao, J.; Swartz, L. A.; Lin, W. F.; Schlenoff, P. S.; Frommer, J.; Schlenoff, J. B.; Liu, G. Y. Three-Dimensional Nanoprinting via Scanning Probe Lithography-Delivered Layer-by-Layer Deposition. *ACS Nano* **2016**, *10* (6), 5656−5662.

(41) Ulman, A. Formation and Structure of Self-Assembled Monolayers. *Chem. Rev.* **1996**, *96* (4), 1533−1554.

(42) Xia, Y.; Rogers, J. A.; Paul, K. E.; Whitesides, G. M. Unconventional Methods for Fabricating and Patterning Nanostructures. *Chem. Rev.* **1999**, *99* (7), 1823−1848.

(43) Gates, B. D.; Xu, Q.; Stewart, M.; Ryan, D.; Willson, C. G.; Whitesides, G. M. New approaches to nanofabrication: molding, printing, and other techniques. *Chem. Rev.* **2005**, *105* (4), 1171−1196.
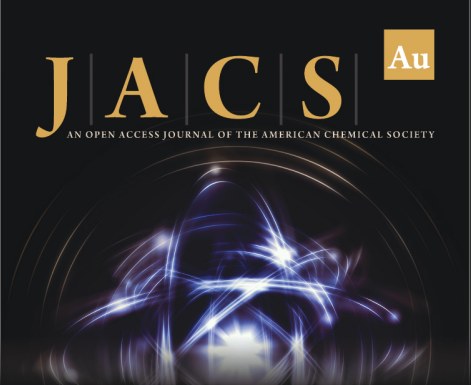
(44) Wen, K.; Maoz, R.; Cohen, H.; Sagiv, J.; Gibaud, A.; Desert, A.; Ocko, B. M. Postassembly chemical modification of a highly ordered organosilane multilayer: new insights into the structure, bonding, and dynamics of self-assembling silane monolayers. *ACS Nano* **2008**, *2* (3), 579−599.

(45) Otte, F. L.; Lemke, S.; Schutt, C.; Krekiehn, N. R.; Jung, U.; Magnussen, O. M.; Herges, R. Ordered monolayers of free-standing porphyrins on gold. *J. Am. Chem. Soc.* **2014**, *136* (32), 11248−11251.

(46) Raigoza, A. F.; Webb, L. J. Molecularly resolved images of peptide-functionalized gold surfaces by scanning tunneling microscopy. *J. Am. Chem. Soc.* **2012**, *134* (47), 19354−19357.

(47) Rosa, L. G.; Liang, J. Atomic force microscope nanolithography: dip-pen, nanoshaving, nanografting, tapping mode, electrochemical and thermal nanolithography. *J. Phys.: Condens. Matter* **2009**, *21* (48), 483001.

(48) Bu, D.; Mullen, T. J.; Liu, G. Y. Regulation of local structure and composition of binary disulfide and thiol self-assembled monolayers using nanografting. *ACS Nano* **2010**, *4* (11), 6863−6873.

(49) Zaba, T.; Noworolska, A.; Bowers, C. M.; Breiten, B.; Whitesides, G. M.; Cyganik, P. Formation of highly ordered self-assembled monolayers of alkynes on Au(111) substrate. *J. Am. Chem. Soc.* **2014**, *136* (34), 11918−11921.

(50) Jung, H.; Kulkarni, R.; Collier, C. P. Dip-pen nanolithography of reactive alkoxysilanes on glass. *J. Am. Chem. Soc.* **2003**, *125* (40), 12096−12097.

(51) Hohman, J. N.; Thomas, J. C.; Zhao, Y.; Auluck, H.; Kim, M.; Vijselaar, W.; Kommeren, S.; Terfort, A.; Weiss, P. S. Exchange reactions between alkanethiolates and alkaneselenols on Au{111}. *J. Am. Chem. Soc.* **2014**, *136* (22), 8110−8121.

(52) Kuramitz, H.; Sugawara, K.; Tanaka, S. Electrochemical sensing of avidin-biotin interaction using redox markers. *Electroanal* **2000**, *12* (16), 1299−1303.

(53) Liu, M.; Zhang, L.; Wang, T. Supramolecular Chirality in Self-Assembled Systems. *Chem. Rev.* **2015**, *115* (15), 7304−7397.

(54) Black, A. L.; Lenhardt, J. M.; Craig, S. L. From molecular mechanochemistry to stress-responsive materials. *J. Mater. Chem.* **2011**, *21* (6), 1655−1663.

(55) Manivannan, M. S.; Silberstein, M. N. Computational investigation of shear driven mechanophore activation at interfaces. *Extreme Mech Lett.* **2016**, *8*, 6−12.

(56) Chen, T.; Yang, W. H.; Wang, D.; Wan, L. J. Globally homochiral assembly of two-dimensional molecular networks triggered by co-absorbers. *Nat. Commun.* **2013**, *4*, 1389.

(57) De Cat, I.; Guo, Z.; George, S. J.; Meijer, E. W.; Schenning, A. P.; De Feyter, S. Induction of chirality in an achiral monolayer at the liquid/solid interface by a supramolecular chiral auxiliary. *J. Am. Chem. Soc.* **2012**, *134* (6), 3171−3177.

(58) Stepanow, S.; Lin, N.; Vidal, F.; Landa, A.; Ruben, M.; Barth, J. V.; Kern, K. Programming supramolecular assembly and chirality in two-dimensional dicarboxylate networks on a Cu(100) surface. *Nano Lett.* **2005**, *5* (5), 901−904.

(59) Vidal, F.; Delvigne, E.; Stepanow, S.; Lin, N.; Barth, J. V.; Kern, K. Chiral phase transition in two-dimensional supramolecular assemblies of prochiral molecules. *J. Am. Chem. Soc.* **2005**, *127* (28), 10101−10106.

(60) Ernst, K. H. Molecular chirality at surfaces. *Physica Status Solidi B-Basic Solid State Physics* **2012**, *249* (11), 2057−2088.

(61) Vettiger, P.; Despont, M.; Drechsler, U.; Durig, U.; Haberle, W.; Lutwyche, M. I.; Rothuizen, H. E.; Stutz, R.; Widmer, R.; Binnig, G. K. The "Millipede"—More than thousand tips for future AFM storage. *IBM J. Res. Dev.* **2000**, *44* (3), 323−340.

(62) Deng, W. N.; Wang, S.; Ventrici de Souza, J.; Kuhl, T. L.; Liu, G.-y. New Algorithm to Enable Construction and Display of 3D Structures from Scanning Probe Microscopy Images Acquired Layer-by-Layer. The. *J. Phys. Chem. A* **2018**, *122* (26), 5756−5763.

(63) Ventrici de Souza, J.; Liu, Y.; Wang, S.; Dörig, P.; Kuhl, T. L.; Frommer, J.; Liu, G.-y. Three-dimensional nanoprinting via direct delivery. The. *J. Phys. Chem. B* **2018**, *122* (2), 956−962.